Research in Astron. Astrophys. **2013** Vol. **13** No. **6**, 641–650
http://www.raa-journal.org *http://www.iop.org/journals/raa*

***R**esearch in*
***A**stronomy and*
***A**strophysics*

The redshift number density evolution of Mg II absorption systems *

Zhi-Fu Chen

Department of Physics and Telecommunication Engineering, Baise University, Baise 533000, China; *zhichenfu@126.com*
Center for Astrophysics, Guangzhou University, Guangzhou 510006, China

Received 2012 May 24; accepted 2013 January 21

Abstract We make use of the recent large sample of 17 042 Mg II absorption systems from Quider et al. to analyze the evolution of the redshift number density. Regardless of the strength of the absorption line, we find that the evolution of the redshift number density can be clearly distinguished into three different phases. In the intermediate redshift epoch ($0.6 \lesssim z \lesssim 1.6$), the evolution of the redshift number density is consistent with the non-evolution curve, however, the non-evolution curve over-predicts the values of the redshift number density in the early ($z \lesssim 0.6$) and late ($z \gtrsim 1.6$) epochs. Based on the invariant cross-section of the absorber, the lack of evolution in the redshift number density compared to the non-evolution curve implies the galaxy number density does not evolve during the middle epoch. The flat evolution of the redshift number density tends to correspond to a shallow evolution in the galaxy merger rate during the late epoch, and the steep decrease of the redshift number density might be ascribed to the small mass of halos during the early epoch.

Key words: methods: statistical — galaxies: evolution — quasars: absorption lines

1 INTRODUCTION

An absorption line can be observed in quasar spectra when the quasar sight line passes through the foreground object, which provides a sensitive probe of otherwise invisible objects or gaseous structures in the universe. Depending on the components and the physical conditions of the absorbing gas, different elements and transitions are expected to show different profiles and strengths. The $\mathrm{Mg\ II}\ \lambda\lambda 2796, 2803$ doublet is commonly seen and has easily identifiable features in quasar spectra, which are believed to originate in photoionized gas with temperature $T \sim 10^4$ K (Bergeron & Stasińska 1986; Charlton et al. 2003) that traces clouds with high column density (Rao et al. 2006).

Although the physical origin of the Mg II absorption systems is unclear, including absorption systems that originate in starburst-driven outflows from nearby star forming regions, which are common in distant galaxies, infalling clouds, or a combination thereof, imaging surveys along quasar sight lines indicate that the great majority of the Mg II absorption systems are associated with galaxies (e.g., Steidel et al. 1994; Kacprzak et al. 2010; Chen et al. 2010). Therefore, the Mg II absorption lines are usually used for investigating the properties of gaseous regions associated with galaxies.

∗ Supported by the National Natural Science Foundation of China.

Based on these Mg II absorption lines, we can better understand outflows arising from star formation and supernovae (e.g., López & Chen 2012; Ménard et al. 2011; Norman et al. 1996; Bond et al. 2001; Nestor et al. 2011), galactic halos/disks (e.g., Charlton & Churchill 1996), the environments around background quasars (e.g., Bowen et al. 2006), and so on.

The utility of Mg II absorption systems has led to many groups to conduct systematic surveys of Mg II absorption features in quasar spectra. The earlier surveys only contained a few quasar spectra (e.g., Weymann et al. 1979; Lanzetta et al. 1987; Tytler et al. 1987; Sargent et al. 1988; Caulet 1989). Lanzetta et al. (1987) analyzed the statistical properties of the Mg II absorption systems at relatively high redshifts ($1.25 < z < 2.15$). The evolution of the number density for absorbers was presented in their work. For Mg II absorption systems at lower redshifts ($0.2 \lesssim z \lesssim 1.5$), Tytler et al. (1987) and Sargent et al. (1988) found that the evolution of the redshift number density agrees with the non-evolution curve that is caused by cosmic expansion. For Mg II absorption systems with a broader redshift range ($0.23 \leqslant z \leqslant 2.06$), Steidel & Sargent (1992) found that the redshift number densities of relatively weak absorption lines do not evolve with cosmic time compared to the non-evolution curve, however, the non-evolution curve over-predicts the redshift number density of the strongest absorption lines at low redshifts.

With the advent of the larger Sloan Digital Sky Survey (SDSS; York et al. 2000), a huge increase in the number of quasar spectra has been archived, and large samples of absorbers are available (e.g., Bouché et al. 2004; Nestor et al. 2005; Prochter et al. 2006; York et al. 2006; Lundgren et al. 2009; Quider et al. 2011). Nestor et al. (2005) made use of the quasar spectra in the SDSS early data release (EDR) (~ 3700 quasars) to investigate the statistical properties of Mg II absorption systems (about 1300 absorption systems). They found that the evolution of redshift number densities parallels cosmic expansion (non-evolution curve) for relatively weak absorption lines, namely the lines with $W_0^{\lambda 2796} \geq 0.3,\ 0.6,\ 1.0,$ and 1.5 Å. However, the redshift number densities of the relatively strong lines evolve with redshift compared to the non-evolution curve, namely the lines with $W_0^{\lambda 2796} \geq 2.0,\ 2.5,\ 3.0$ and 3.5 Å.

In this paper, we will utilize the recent large sample of 17 042 Mg II absorption systems to revise the evolution of the redshift number density of absorbers, which was constructed using quasar spectra by Quider et al. (2011) from SDSS Data Release 4 (DR4). The paper is organized as follows. Section 2 presents the origin of the data and the redshift path. In Section 3 we show the distributions of redshift number density and make a comparison with the predictions of the non-evolution curve. Section 4 has a discussion and conclusions. Throughout this paper, we adopt a *WMAP* cosmology with $\Omega_{\rm m} = 0.274$ and $H_0 = 70.2$ km s^{-1} Mpc^{-1} (Komatsu et al. 2011).

2 MG II ABSORPTION SYSTEMS

The Mg II $\lambda\lambda 2796, 2803$ absorption lines can be detected in the SDSS quasar spectra over the redshift range $0.4 \lesssim z \lesssim 2.2$. In this paper, we make use of the Pittsburgh SDSS Mg II Absorption-Line Survey Catalog, which was constructed by Quider et al. (2011) using the method of Nestor et al. (2005). Quider et al. (2011) utilized a combination of cubic splines and Gaussians to produce continua fits, including the true continuum, emission and absorption features. They searched for Mg II $\lambda\lambda 2796, 2803$ absorption lines in the continuum-normalized SDSS quasar spectra, and applied an optimal extraction method and a Gaussian line profile to measure each rest equivalent width W_0. All the candidate Mg II doublets were visually checked to determine their validity. The $\lambda 2796$ rest equivalent width detection limit $W_0^{\rm lim}$ was calculated by determining the 1σ theoretical error of the rest equivalent width. We refer the reader to Nestor et al. (2005) and Quider et al. (2011) for more details.

Figure 1 shows the distribution of absorption redshifts for all the 17 042 systems from Quider et al. (2011).

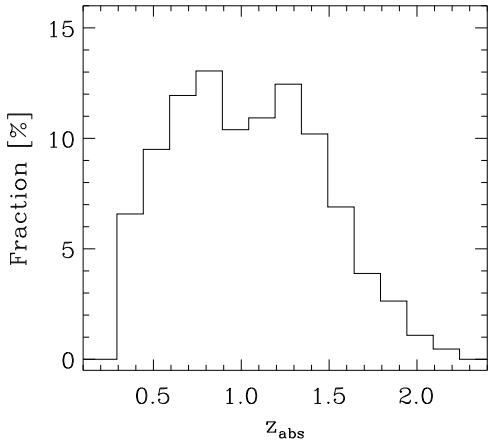

Fig. 1 Distribution of absorption redshifts for all 17 042 systems from Quider et al. (2011).

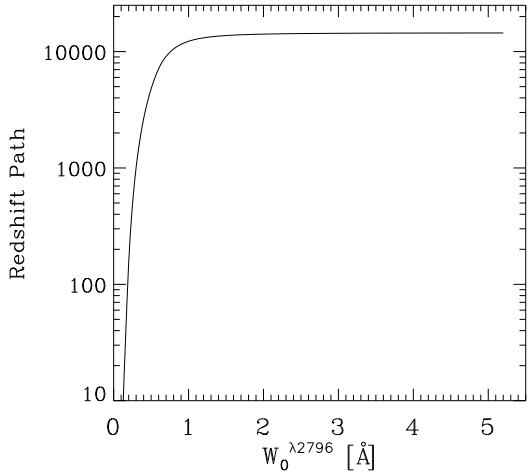

Fig. 2 Redshift path covered by the Pittsburgh SDSS Mg II Absorption-Line Survey Catalog, shown as a function of $\mathrm{W}_0^{\lambda 2796}$.

The total redshift path covered by the Pittsburgh SDSS Mg II Absorption-Line Survey Catalog for each value of $\mathrm{W}_0^{\lambda 2796}$ is given by

$$\Delta Z(W_0^{\lambda 2796}) = \int_{z_{\min}}^{z_{\max}} \sum_{i=1}^{N_{\rm spec}} g_i(W_0^{\lambda 2796}, z) dz. \quad (1)$$

Here, $g_i(W_0^{\lambda 2796}, z) = 1$ for $W_0^{\rm lim}(z) \leq W_0^{\lambda 2796}$ and $g_i(W_0^{\lambda 2796}, z) = 0$ otherwise. The redshift limits are defined to be $3000\,{\rm km\,s^{-1}}$ above the $\mathrm{Ly}\alpha\ \lambda 1216$ emission line and $3000\,{\rm km\,s^{-1}}$ below the $\mathrm{Mg\ II}\ \lambda 2800$ emission line, or the limits of the spectra. The redshift coverage is plotted in Figure 2.

Table 1 $\partial N/\partial z$ Results for $W_0^{\lambda 2796}$–Limited Samples

z bin	Equivalent width limit ($W_0^{\rm lim}$) of $W_0^{\lambda 2796} \geq W_0^{\rm lim}$							
	$\partial N/\partial z$							
± 0.05	0.2Å	0.6Å	0.8Å	1.2Å	1.8Å	2.5Å	3.0Å	3.5Å
0.3674	0.0765	0.0482	0.0376	0.0250	0.0111	0.0025	0.0008	0.0002
0.4674	0.1077	0.0642	0.0507	0.0286	0.0110	0.0032	0.0013	0.0006
0.5674	0.1466	0.0815	0.0611	0.0344	0.0147	0.0056	0.0017	0.0004
0.6674	0.1717	0.0949	0.0731	0.0406	0.0161	0.0065	0.0031	0.0011
0.7674	0.1916	0.1045	0.0804	0.0451	0.0178	0.0070	0.0036	0.0019
0.8674	0.1901	0.1028	0.0781	0.0424	0.0173	0.0057	0.0022	0.0007
0.9674	0.1397	0.0894	0.0699	0.0433	0.0203	0.0074	0.0033	0.0016
1.0674	0.1214	0.0806	0.0653	0.0434	0.0194	0.0074	0.0038	0.0015
1.1674	0.1610	0.0881	0.0683	0.0399	0.0161	0.0067	0.0037	0.0019
1.2674	0.1894	0.0972	0.0734	0.0395	0.0163	0.0062	0.0028	0.0011
1.3674	0.1604	0.0918	0.0696	0.0397	0.0171	0.0071	0.0036	0.0020
1.4674	0.1548	0.0830	0.0622	0.0336	0.0159	0.0067	0.0039	0.0023
1.5674	0.0986	0.0566	0.0464	0.0282	0.0147	0.0063	0.0034	0.0014
1.6674	0.0708	0.0460	0.0378	0.0236	0.0111	0.0047	0.0024	0.0007
1.7674	0.0377	0.0291	0.0252	0.0174	0.0085	0.0036	0.0015	0.0008
1.8674	0.0334	0.0274	0.0234	0.0150	0.0079	0.0032	0.0016	0.0009
1.9674	0.0140	0.0130	0.0118	0.0089	0.0048	0.0020	0.0010	0.0006
2.0674	0.0072	0.0069	0.0059	0.0049	0.0030	0.0013	0.0007	0.0006
2.1674	0.0049	0.0043	0.0039	0.0033	0.0025	0.0012	0.0005	0.0003
N_0 [a]:	0.0663	0.0334	0.0254	0.0144	0.0061	0.0024	0.0012	0.0006
Prob [b]:	0.0486	0.1161	0.1161	0.2467	0.2467	0.1161	0.0486	0.0060
Prob [c]:	0.0036	0.0026	0.0032	0.0056	0.0122	0.0099	0.0037	0.0019

Notes — a: N_0 represents the normalization factor of Equation (6) with $\varepsilon = 0$, which is determined from the minimum χ^2 fitting of the measured $\partial N/\partial z$ using Equation (6) with $\varepsilon = 0$. b: The probability of the K-S test, for which a small value shows that the distribution of the measured $\partial N/\partial z$ is significantly different from that of the prediction of no evolution. c: The probability of the F-Test, for which a small value (less than 0.05) indicates that two distributions are significantly different.

3 EVOLUTION IN THE REDSHIFT NUMBER DENSITY

The incidence of lines, $\partial N/\partial z$, namely redshift number density, is the number of absorbers per unit redshift path in an interval of $W_0^{\lambda 2796}$, which is given by

$$\frac{\partial N}{\partial z} = \sum_{i=1}^{N_{\rm abs}} \frac{1}{\Delta Z(W_0^i)}, \tag{2}$$

where the sum is over the systems with W_0^i, and $N_{\rm abs}$ represents the number of absorbers in the given interval. The variance of the incidence of lines is defined as

$$\sigma^2_{\partial N/\partial z} = \sum_{i=1}^{N_{\rm abs}} \left[\frac{1}{\Delta Z(W_0^i)}\right]^2. \tag{3}$$

Historically, this analysis has focused on $\partial N/\partial z$ as a function of redshift for lines within a specified equivalent width interval. We compute $\partial N/\partial z$ as a function of redshift for $W_0^{\lambda 2796} \geq 0.2,\ 0.6,\ 0.8,\ 1.2,\ 1.8,\ 2.5,\ 3.0$ and 3.5 Å.

The results are provided in Table 1 and presented in Figure 3. As mentioned in Nestor et al. (2005) and Quider et al. (2011), a dip at $z \approx 1.1$ for the subsamples with small equivalent width limits are due to the ubiquitous decrease in the signal to noise ratio (S/N) at the wavelength that corresponds to the split between the blue-side and red-side cameras (Stoughton et al. 2002).

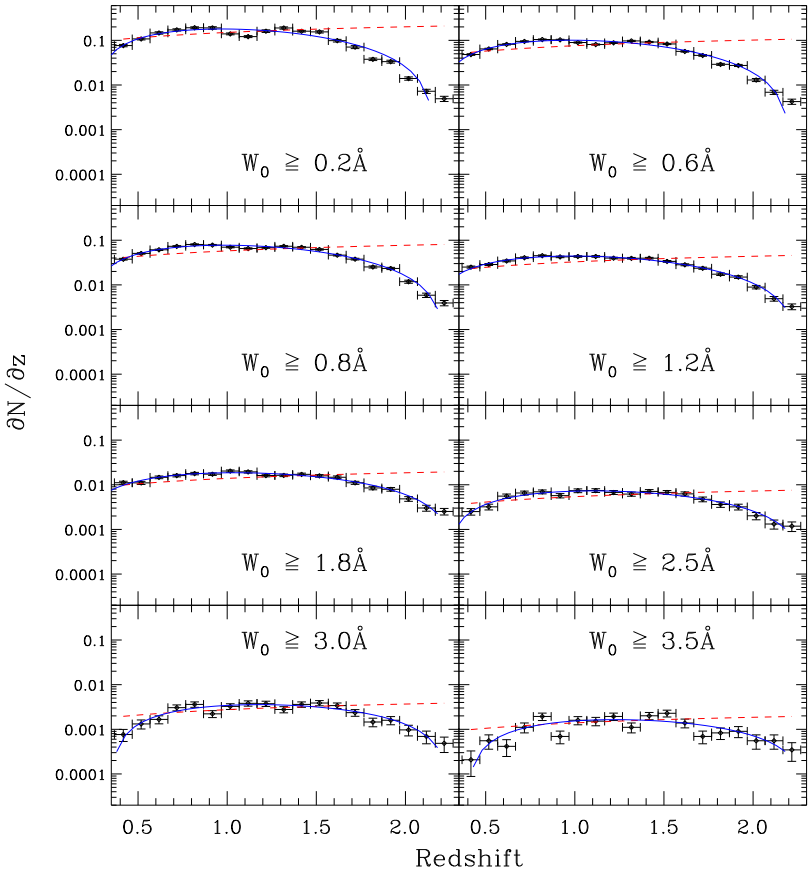

Fig. 3 Evolution in the redshift number density of Mg II absorbers for $W_0^{\lambda 2796} \geq W_0^{\rm lim}$ subsamples. The dashed lines represent the non-evolution curves, which are normalized to minimize the χ^2 to the measured $\partial N/\partial z$. The solid lines represent the best χ^2 fits to the polynomial linear function, namely $\partial N/\partial z = a + bz + cz^2 + dz^3$.

The evolution of $\partial N/\partial z$ is influenced by the expansion of the universe. The redshift number density, $\partial N/\partial z$, is associated with a cosmological model and describes the number of absorbers per co-moving path length, which is usually expressed as

$$\frac{\partial N}{\partial z} = \frac{c}{H_0} n(z)\sigma(z)\frac{dX}{dz} = N(z)\frac{(1+z)^2}{\sqrt{\Omega_M(1+z)^3+\Omega_\Lambda}} \tag{4}$$

for the concordance cosmological model. Here $N(z) = (c/H_0)n(z)\sigma(z)$, $n(z)$ is the number density of absorbers and $\sigma(z)$ represents the geometric cross-section of the absorber. Generally speaking, assuming

$$N(z) = \frac{c}{H_0} n_0 \sigma_0 (1+z)^{\varepsilon} \tag{5}$$

to parameterize the evolution of $n(z)\sigma(z)$, then

$$\frac{\partial N}{\partial z} = N_0 \frac{(1+z)^{2+\varepsilon}}{\sqrt{\Omega_M(1+z)^3+\Omega_\Lambda}}. \tag{6}$$

Here, $N_0 = (c/H_0)n_0\sigma_0$, which does not evolve with redshift, and ε is the evolution parameter. N_0 and ε are usually determined by the measured $\partial N/\partial z$. If $\varepsilon = 0$, $N(z)$ corresponds to the case of non-evolution. Thus, $\partial N/\partial z$ increases with increasing redshift, which is due to the expansion of the universe for the non-evolution case.

One can compare the values of the measured $\partial N/\partial z$ to those of the predictions of *the non-evolution curve* (Eq. (6) with $\varepsilon = 0$). In order to determine the normalization factor N_0, we invoke Equation (6), assuming $\varepsilon = 0$, to fit the data of the measured $\partial N/\partial z$ by minimizing the χ^2 value. The fitted values of N_0 are presented in Table 1. For each limited equivalent width subsample over the whole redshift range, we apply the Kolmogorov-Smirnov Test (K-S Test) to the values of the measured $\partial N/\partial z$ and the predictions of the non-evolution curves. The probabilities (a small probability indicates that the two distributions are drawn from different populations) of the K-S Test are also provided in Table 1. The probabilities of the K-S Test for the $W_0^{\lambda 2796} \geq 0.6,\ 0.8,\ 1.2,\ 1.8$ and 2.5 Å subsamples do not reject the hypothesis that the values of the measured $\partial N/\partial z$ are similar to those of the predictions of the non-evolution curve, even though the deviations of the two distributions are large at high redshifts. For the $W_0^{\lambda 2796} \geq 0.2,\ 3.0$ and 3.5 Å subsamples, the non-evolution curves over-predict the values of $\partial N/\partial z$ at low and high redshifts. However, the F-variance Test (F-Test) supports the conclusion that the values of the measured $\partial N/\partial z$ and the predictions of non-evolution curves differ significantly from each other for each limited equivalent subsample. The results of the F-Test were not supported by either Steidel & Sargent (1992) or Nestor et al. (2005), who reported that the values of the measured $\partial N/\partial z$ are formally in agreeable with those of the predictions of the non-evolution curves for the subsamples having small equivalent width limits.

As mentioned above, here we consider the influence of the expansion of the universe, and try to describe the evolution of the values of the measured $\partial N/\partial z$ with redshift using the form of Equation (6). However, this functional form cannot fit the values of the measured $\partial N/\partial z$ very well, which also occurs in the power-law functional form $N_0(1+z)^\gamma$. This evidence demonstrates that the evolution of $\partial N/\partial z$ is complex and cannot be well described with a single power-law for any given limited equivalent width sample, which was also the conclusion of Storrie-Lombardi & Wolfe (2000). Prochter et al. (2006) found that the exponential functional form $N\exp(-z_0/z)$ describes the values of $\partial N/\partial z$ well. However, we stress that this functional form also cannot model our data very well. In particular, this functional form cannot describe the declines of $\partial N/\partial z$ at high redshifts. Here we also consider the simple linear functional form $a + bz$, which was also used by Prochter et al. (2006) but this form could represent their data very well. This simple linear functional form also cannot represent our data either. Therefore, we invoke the more complex linear functional form, namely $\partial N/\partial z = a+bz+cz^2+dz^3$, to fit the values of the measured $\partial N/\partial z$. The fitting results are plotted in Figure 3 with blue lines, which indicate that the complex linear functional form is indeed a good description to the data.

Due to the sizable data sample, we are able to analyze the distributions of $\partial N/\partial z$ for ranges of $W_0^{\lambda 2796}$. This is very important, since different absorption strengths of the lines may exhibit different behaviors of evolution. Therefore, we repeat the above processes for the following equivalent width ranges: 0.2 Å $\leq W_0^{\lambda 2796} < 0.6$ Å, 0.6 Å $\leq W_0^{\lambda 2796} < 0.8$ Å, 0.8 Å $\leq W_0^{\lambda 2796} < 1.2$ Å, 1.2 Å $\leq W_0^{\lambda 2796} < 1.8$ Å, 1.8 Å $\leq W_0^{\lambda 2796} < 2.5$ Å, 2.5 Å $\leq W_0^{\lambda 2796} < 3.0$ Å and $W_0^{\lambda 2796} \geq 3.5$ Å.

The results are displayed in Figure 4 and presented in Table 2. The normalization factors N_0 (the fitted results using Equation (6) with $\varepsilon = 0$), and the probabilities of the K-S Test and the F-Test are also provided in Table 2. Except for the subsamples where 0.2 Å $\leq W_0^{\lambda 2796} < 0.6$ Å, and $W_0^{\lambda 2796} \geq 3.5$ Å, the probabilities of the K-S Test do not reject the hypothesis that the two distributions are similar. This evidence was also presented by Nestor et al. (2005). However, the F-Test does not support the conclusion that the values of the measured $\partial N/\partial z$ are consistent with those of the predictions of the non-evolution curve for each subsample. The exponential function, a single power-law function, the simple linear function, and the form of Equation (6) also cannot

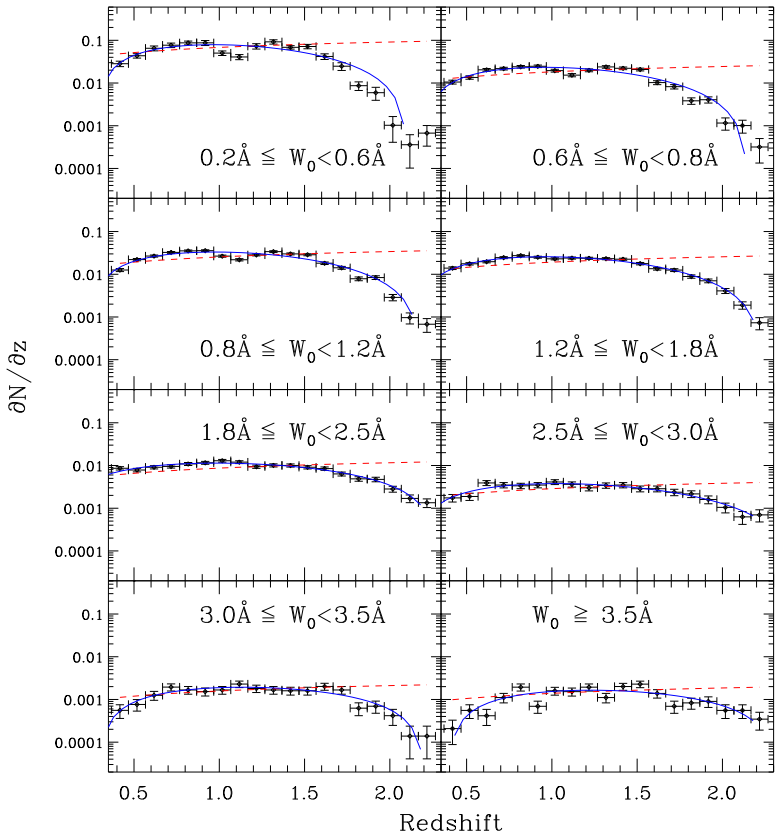

Fig. 4 Evolution of the redshift number density of Mg II absorbers for ranges of $W_0^{\lambda 2796}$ subsamples. The dashed lines represent the non-evolution curves, which are normalized to minimize the χ^2 to the measured $\partial N/\partial z$. The solid lines represent the best χ^2 fits to the polynomial linear function, namely $\partial N/\partial z = a + bz + cz^2 + dz^3$. The measured ∂N$/\partial$z departure from the polynomial linear function is due to the dip at $z \approx 1.1$ for the ubiquitous decline in S/N with wavelength.

well represent the true distribution of $\partial N/\partial z$. The polynomial linear function is also invoked to fit the values of the measured ∂N$/\partial$z, which are plotted in Figure 4 with blue lines. Except for the subsamples where 0.2 Å $\leq W_0^{\lambda 2796} < 0.6$ Å, 0.6 Å $\leq W_0^{\lambda 2796} < 0.8$ Å and 0.8 Å $\leq W_0^{\lambda 2796} < 1.2$ Å, which ascribe the obvious dips at $z \approx 1.1$ to the ubiquitous decline in S/N with wavelength, the distributions are very consistent with the curves of the polynomial linear function.

4 DISCUSSION AND CONCLUSIONS

The exponential function, simple linear function and single power-law function cannot describe $\partial N/\partial z$ well. Only the polynomial linear function is adequate, which reveals that the evolution of $\partial N/\partial z$ is somewhat complex. The influence of dichroic mainly acts *on the weak lines* (see fig. 8 of Nestor et al. 2005 for details). Ignoring the influence of the dichroic, $\partial N/\partial z$ is nearly a constant at intermediate redshifts ($0.6 \lesssim z \lesssim 1.6$) for each subsample shown in Figures 3 and 4, which can be well described with a simple linear function ($\partial N/\partial z = a + bz$). However, $\partial N/\partial z$ shallowly increases with increasing redshifts at low-end values ($z \lesssim 0.6$), and steeply declines with increasing

Table 2 $\partial N/\partial z$ Results for $W_0^{\lambda 2796}$–Limited Samples

z bin	Equivalent width limit ($W_0^{\rm lim}$) of $W_0^{\lambda 2796} \geq W_0^{\rm lim}$ [Å]							
	$\partial N/\partial z$							
± 0.05	[0.2,0.6)	[0.6,0.8)	[0.8,1.2)	[1.2,1.8)	[1.8,2.5)	[2.5,3.0)	[3.0,3.5)	$[3.5,\infty)$
0.3674	0.0283	0.0106	0.0126	0.0139	0.0086	0.0017	0.0006	0.0002
0.4674	0.0435	0.0135	0.0221	0.0176	0.0078	0.0019	0.0008	0.0006
0.5674	0.0651	0.0204	0.0267	0.0197	0.0091	0.0039	0.0013	0.0004
0.6674	0.0768	0.0218	0.0325	0.0245	0.0095	0.0035	0.0019	0.0011
0.7674	0.0872	0.0241	0.0353	0.0273	0.0109	0.0033	0.0017	0.0019
0.8674	0.0873	0.0247	0.0357	0.0251	0.0116	0.0035	0.0015	0.0007
0.9674	0.0502	0.0195	0.0266	0.0230	0.0129	0.0041	0.0017	0.0016
1.0674	0.0408	0.0153	0.0219	0.0240	0.0120	0.0036	0.0023	0.0015
1.1674	0.0728	0.0199	0.0284	0.0237	0.0094	0.0030	0.0018	0.0019
1.2674	0.0922	0.0239	0.0339	0.0232	0.0101	0.0034	0.0017	0.0011
1.3674	0.0686	0.0222	0.0300	0.0225	0.0100	0.0035	0.0016	0.0020
1.4674	0.0718	0.0208	0.0286	0.0178	0.0091	0.0029	0.0016	0.0023
1.5674	0.0419	0.0102	0.0182	0.0135	0.0085	0.0029	0.0020	0.0014
1.6674	0.0248	0.0082	0.0142	0.0125	0.0064	0.0024	0.0017	0.0007
1.7674	0.0087	0.0038	0.0079	0.0089	0.0049	0.0022	0.0006	0.0008
1.8674	0.0059	0.0041	0.0084	0.0070	0.0047	0.0016	0.0007	0.0009
1.9674	0.0010	0.0012	0.0029	0.0041	0.0028	0.0010	0.0004	0.0006
2.0674	0.0004	0.0010	0.0010	0.0019	0.0017	0.0006	0.0001	0.0006
2.1674	0.0007	0.0003	0.0007	0.0007	0.0013	0.0007	0.0001	0.0003
N_0 [a]:	0.0300	0.0080	0.0112	0.0085	0.0038	0.0013	0.0007	0.0006
Prob [b]:	0.0060	0.0486	0.1161	0.1161	0.4622	0.2467	0.1161	0.0060
Prob [c]:	0.0013	0.0011	0.0014	0.0030	0.0111	0.0068	0.0049	0.0019

Notes: see Table 1 for the meanings of N_0 and probabilities associated with the K-S and F tests.

redshifts at high-end values ($z \gtrsim 1.6$). These three different behaviors of evolution are more obvious for stronger lines.

The evolutions of $\partial N/\partial z$ shown in Figures 3 and 4 differ significantly from those of Nestor et al. (2005) (see their figs. 9 and 10). Nestor et al. found that there is no evolution at most redshifts for the relatively weak systems ($W_0 < 2.0$ Å), but for the relatively strong systems ($W_0 > 2.0$ Å), the values of $\partial N/\partial z$ increase significantly toward high redshifts. They also found that the distributions of $\partial N/\partial z$ are almost consistent with the non-evolution curve, regardless of the W_0 value. Here we restrict the Mg II absorption systems to the quasars in SDSS EDR, which were used by Nestor et al. (2005), and again analyze the distributions of $\partial N/\partial z$. We find that our results (the distributions of $\partial N/\partial z$) are consistent with those of Nestor et al. when restricting the Mg II absorption systems to the quasars in SDSS EDR. Therefore, we suspect that the differences between our results (our Figs. 3 and 4) and those of Nestor et al. (2005) (their figs. 9 and 10) might arise from the sample sizes.

It can be noticed from the distribution of Mg II absorption systems (see Fig. 1) that the detected numbers of absorption systems markedly decline at $z \gtrsim 1.6$ and at $z \lesssim 0.6$. One would suspect that the declines of $\partial N/\partial z$ shown in Figures 3 and 4 should arise from the remarkable decline in the detected numbers of absorption systems. Here we apply the K-S test to the distributions of $\partial N/\partial z$ (shown in Fig. 4) and the detected numbers of absorption systems in the same redshift bins. The probabilities of the K-S test are provided in Table 3. Except for the sample where $0.2\ \text{Å} \leq W_0^{\lambda 2796} < 0.6\ \text{Å}$, the probabilities of the K-S test imply that the distributions of $\partial N/\partial z$ are not determined by the detected numbers of absorption systems.

The Mg II absorbers are nearly always associated with galaxies (e.g., Bergeron 1986; Kacprzak et al. 2008). The number density of galaxies with $M > M_*(z = 2) \approx 10^{11} M_\odot$ evolves with redshift with an exponential form in the middle epoch (e.g., Jenkins et al. 2001). The $\partial N/\partial z$ values shown in Figures 3 and 4 are nearly a constant at intermediate redshifts ($0.6 \lesssim z \lesssim 1.6$), which imply that the cross-sections of absorbers, if they are determined by the massive galaxies, decline exponentially.

Table 3 Probabilities of the K-S test for the distributions of $\partial N/\partial z$ and the detected numbers of absorption systems.

$W_0^{\lambda 2796}$ range [Å]	[0.2,0.6)	[0.6,0.8)	[0.8,1.2)	[1.2,1.8)	[1.8,2.5)	[2.5,3.0)	[3.0,3.5)	$[3.5,\infty)$
Probability	0.74	2.27E–5	1.09E–4	2.27E–5	1.03E–7	1.34E–8	1.57E–9	1.57E–9

Such parallel evolutions are highly improbable. Moreover, the anti-correlation between the observed $W_0^{\lambda 2796}$ and the projected distance. There ρ (e.g., Chen et al. 2010) indicates that the cross-section of the absorber with respect to $W_0^{\lambda 2796}$ is nearly constant. Therefore, it is more reasonable that the almost constant $\partial N/\partial z$ is related to the galaxy number density and to the cross-section showing no evolution during this epoch.

As noted above, $\partial N/\partial z$ shows a flat evolution in the late epoch, which is also expected for the galaxy merger rate (Lin et al. 2004). As long as one assumes that the Mg II absorbers are closely related to the starbursts (Bond et al. 2001) and the starburst is driven by a galaxy merger, combined with the invariant cross-section of the absorber, the merger of galaxies would mainly contribute to the decrease of $\partial N/\partial z$ in the late epoch.

Tinker & Chen (2008) presented a model which shows that the Mg II absorbers are related to the mass of dark matter halos. In their model, most of the Mg II absorbers reside in the halos with $M_h = 10^{11.5} \sim 10^{12.5}\ h^{-1}\ M_\odot$. The incidence rate of Mg II absorption systems declines rapidly in halos with lower mass. In the early epoch, the mass of the dark matter halo would be too low to produce Mg II absorption lines with enough strength. The infalling gas outside of the halo increases the mass of the dark matter halo, which ensures that the halo has sufficient cold gas to produce the Mg II absorption lines with enough strength in the early epoch. The steep decreases of $\partial N/\partial z$ at high redshifts might mainly be ascribed to the smaller mass of the halo in the early epoch.

Acknowledgements We thank the anonymous referees for their helpful comments and suggestions that greatly improved this paper. This work was supported by the National Natural Science Foundation of China (No. 11073007), the Guangzhou technological project (No. 11C62010685), and Guangxi Natural Science Foundation (2012jjAA10090).

References

Bergeron, J. 1986, A&A, 155, L8
Bergeron, J., & Stasińska, G. 1986, A&A, 169, 1
Bond, N. A., Churchill, C. W., Charlton, J. C., & Vogt, S. S. 2001, ApJ, 562, 641
Bouché, N., Murphy, M. T., & Péroux, C. 2004, MNRAS, 354, L25
Bowen, D. V., Hennawi, J. F., Ménard, B., et al. 2006, ApJ, 645, L105
Caulet, A. 1989, ApJ, 340, 90
Charlton, J. C., & Churchill, C. W. 1996, ApJ, 465, 631
Charlton, J. C., Ding, J., Zonak, S. G., et al. 2003, ApJ, 589, 111
Chen, H.-W., Helsby, J. E., Gauthier, J.-R., et al. 2010, ApJ, 714, 1521
Jenkins, A., Frenk, C. S., White, S. D. M., et al. 2001, MNRAS, 321, 372
Kacprzak, G. G., Churchill, C. W., Steidel, C. C., & Murphy, M. T. 2008, AJ, 135, 922
Kacprzak, G. G., Churchill, C. W., Ceverino, D., et al. 2010, ApJ, 711, 533
Komatsu, E., Smith, K. M., Dunkley, J., et al. 2011, ApJS, 192, 18
Lanzetta, K. M., Turnshek, D. A., & Wolfe, A. M. 1987, ApJ, 322, 739
Lin, L., Koo, D. C., Willmer, C. N. A., et al. 2004, ApJ, 617, L9
López, G., & Chen, H.-W. 2012, MNRAS, 419, 3553
Lundgren, B. F., Brunner, R. J., York, D. G., et al. 2009, ApJ, 698, 819
Ménard, B., Wild, V., Nestor, D., et al. 2011, MNRAS, 417, 801

Nestor, D. B., Turnshek, D. A., & Rao, S. M. 2005, ApJ, 628, 637
Nestor, D. B., Johnson, B. D., Wild, V., et al. 2011, MNRAS, 412, 1559
Norman, C. A., Bowen, D. V., Heckman, T., Blades, C., & Danly, L. 1996, ApJ, 472, 73
Prochter, G. E., Prochaska, J. X., & Burles, S. M. 2006, ApJ, 639, 766
Quider, A. M., Nestor, D. B., Turnshek, D. A., et al. 2011, AJ, 141, 137
Rao, S. M., Turnshek, D. A., & Nestor, D. B. 2006, ApJ, 636, 610
Sargent, W. L. W., Steidel, C. C., & Boksenberg, A. 1988, ApJ, 334, 22
Steidel, C. C., & Sargent, W. L. W. 1992, ApJS, 80, 1
Steidel, C. C., Dickinson, M., & Persson, S. E. 1994, ApJ, 437, L75
Storrie-Lombardi, L. J., & Wolfe, A. M. 2000, ApJ, 543, 552
Stoughton, C., Lupton, R. H., Bernardi, M., et al. 2002, AJ, 123, 485
Tinker, J. L., & Chen, H.-W. 2008, ApJ, 679, 1218
Tytler, D., Boksenberg, A., Sargent, W. L. W., Young, P., & Kunth, D. 1987, ApJS, 64, 667
Weymann, R. J., Williams, R. E., Peterson, B. M., & Turnshek, D. A. 1979, ApJ, 234, 33
York, D. G., Adelman, J., Anderson, J. E., Jr., et al. 2000, AJ, 120, 1579
York, D. G., Khare, P., Vanden Berk, D., et al. 2006, MNRAS, 367, 945